

Patterned Enteroscopy Balloon Design Factors Influence Tissue Anchoring

Leah K. Bowen, Karl Johannes, Emily Zuetell, Kristin N. Calahan, Steven A. Edmundowicz, Rong Long, and Mark E. Rentschler

Abstract

Balloon-assisted enteroscopy procedures allow visualization and intervention in the small intestine. These balloons anchor an endoscope and/or overtube to the small intestine, allowing endoscopists to plicate the small intestine over the overtube. This procedure can extend examination deeper into the small intestine than the length of the endoscope would allow with direct examination. However, procedures are often prolonged or incomplete due to balloon slippage. Enteroscopy balloons are pressure-limited to ensure patient safety and thus, improving anchoring without increasing pressure is essential. Patterning balloon exteriors with discrete features may enhance anchoring at the tissue-balloon interface. Here, the pattern design space is explored to determine factors that influence tissue anchoring. The anchoring ability of smooth versus balloons with patterned features is investigated by experimentally measuring a peak force required to induce slippage of an inflated balloon inside ex-vivo porcine small intestine. Stiffer materials, low aspect-ratio features, and pattern area/location on the balloons significantly increase peak force compared to smooth silicone balloons. Smooth latex balloons, used for standard enteroscopy, have the lowest peak force. This work demonstrates both a method to pattern curved surfaces and that a balloon with patterned features improves anchoring against a deformable, lubricated tissue interface.

1. Introduction

Balloon-assisted enteroscopy is used to diagnose and treat small intestinal diseases including ulcers, obstruction, occult bleeding, and other abnormalities. The small intestine is difficult to navigate using typical endoscopes for two reasons. First, the small intestine can only be reached endoscopically by first navigating through the colon (rectal route) or the esophagus and stomach (oral route). Second, the small intestine is approximately six meters long and often tortuous whereas a traditional endoscope is less than two meters long. In balloon enteroscopy procedures, any portion of the small intestine can be visualized by plicating and compressing the small intestine on the overtube, allowing endoscopic interventions to be performed such as dilation, stenting, hemostasis, polypectomy, biopsy, ablation, and resection[1]. Balloon enteroscopy allows the gastroenterologist to investigate more of the gastrointestinal tract than traditional “push” or direct enteroscopy. It is also interventional unlike capsule enteroscopy which can visualize the entire small intestine but cannot provide therapy or biopsy[2]. Balloon enteroscopy is also less invasive than surgical access[1].

The balloon enteroscopy system includes an endoscope, balloon overtube, and pressure control unit for balloon inflation and deflation. For single balloon enteroscopy, the balloon is attached to the end of the overtube. The endoscope extends through the overtube and the two slide freely against each other. After intubation, the endoscope is operatively advanced as far as possible. The balloon overtube is then advanced to this distal point and the balloon is inflated, anchoring it against the intestinal wall. The balloon overtube is then pulled backwards as the endoscope is advanced further. The endoscope tip then actuates to “hook” the tissue so that the balloon overtube can advance forward again after balloon deflation. As the balloon overtube and endoscope sequentially advance, the small intestine effectively pleats over the overtube and endoscope. Ultimately, this push-pull maneuvering of the balloon overtube interfaced with the intestine allows a two-meter long endoscope to investigate a much longer length of small intestine. For double

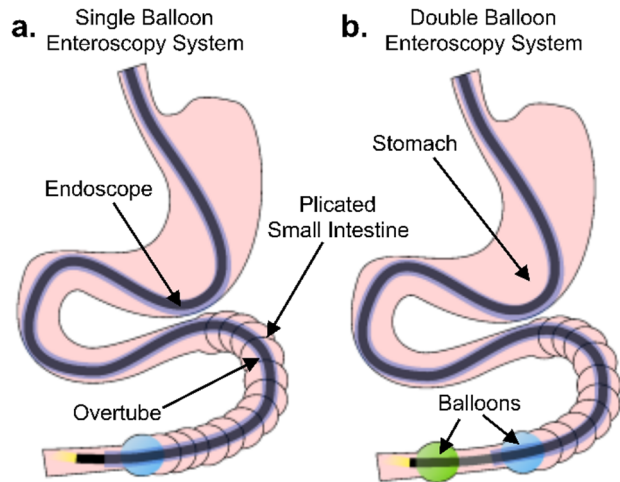


Figure 1. Overview of single and double balloon enteroscopy scope advancement techniques for diagnostic and therapeutic access into the small intestine. (a) In a single balloon enteroscopy procedure, an endoscope and balloon overtube are inserted into the small intestine. The endoscope secures a section of small intestine by hooking it. Then, the overtube is moved distally, pleating the small intestine on the overtube. The balloon, attached to the overtube, is inflated, and holds the pleated small intestine on the overtube. This process is repeated, allowing advancement of the endoscope far into the small intestine and pleating the small intestine on the overtube as shown. (b) In the double balloon procedure, balloons are located on the overtube as well as endoscope tip. Compared to the single balloon procedure, the endoscope balloon secures a section of small intestine. The overtube balloon behaves in a similar manner in both procedures.

an inner layer of mucus central to the mucosa[12], making it difficult to navigate and slippery. The mucus layer is 25-54 μm in pigs [13,14] and is approximately 300 μm thick in the human large intestine[15]. During procedures, these balloon overtubes are pressure limited to prevent over-inflation of balloons. However, this limits the anchoring that can be achieved by increasing pressure. A balloon with enhanced anchoring could reduce costs and significantly improve access to care through more successful procedures and wider procedure adoption. Less balloon slippage would reduce procedure times, physician frustration, and repeat procedures, while leading to an increase in the number of completed procedures, diagnostic findings, and therapeutic success.

In this study, we propose that the addition of patterned features to enteroscopy balloons can improve anchoring of the tissue-balloon interface. Surface patterns have been shown to modulate contact properties, including adhesion and traction, compared to unpatterned or smooth surfaces[16–18]. A large body of literature has shown that some types of soft patterns on relatively stiff substrates have increased adhesion relative to smooth surfaces in dry systems.

Patterned features can increase adhesion and can allow for multiple adhesion cycles during dry adhesion[17,19,20]. When considering a lubricated surface, such as the mucus-coated small intestine, Cheung et al. demonstrated adhesion can be enhanced by using high aspect ratio (height/radius>1), oil-coated, cylindrical patterns when in contact with an aluminum substrate[21]. In addition to affecting adhesion, surface patterns can also increase[22] or decrease friction[23] on dry or wet[24] substrates, depending on pattern geometry. Finally, surface patterns have been applied to new technologies like robotic grippers. Soft gripper patterns such as circumferential ribs[25] and microscopic wedges,[26] have

balloon enteroscopy (DBE), one balloon attaches to the end of the overtube and the other balloon attaches directly to the endoscope near the distal camera end. The only difference in use is that in DBE the endoscope tip does not “hook” tissue, but instead the distal balloon inflates to anchor to the tissue before advancing the trailing balloon overtube (Figure 1)[1,3–5].

Despite the immense benefits, balloon enteroscopy is a technically challenging procedure. One study reported an initial success rate for total endoscopic visualization of the small intestine of only eight percent for an endoscopist with 15 years of endoscopic practice[6]. Another study revealed that DBE procedures performed by experienced endoscopists had a 31% failure rate when advanced via a rectal route[7]. Additionally, both studies estimated the average procedure time for DBE to be over 90 minutes[6,7], compared to 20-40 minutes for a colonoscopy[8]. These lengthy and often incomplete procedures are frequently a result of slippage between the balloons used and the mucosal lining of the GI tract[9–11]. Small intestine anatomy is a contributing factor to this difficulty. The small intestine is convoluted and has

demonstrated improved adhesion over unpatterned grippers[27].

However, less literature exists on the effects of patterns in contact with soft and/or wet surfaces such as the balloon-tissue interface. Assenbergh et al. showed microscale polydimethylsiloxane (PDMS) dimples have greater adhesion compared to smooth PDMS on 12 kPa polyvinyl alcohol (PVA) but not stiffer 18 kPa PVA[28]. McGhee et al. have discussed adhesive mechanisms of dehydrated gel adhesion to mucin. Mucin may transfer onto dehydrated gels, increasing adhesion[29]. Two studies of effects of size on cylindrical PDMS features found that a 70 μm radius increases friction relative to larger and smaller feature radii on intestinal tissues. Kwon et al. measured frictional force of patterned features against a cleaned porcine small intestine while varying normal force, lubricating silicone oil viscosity, and features size[30]. Zhang et al. measured coefficient of friction of patterned features on rabbit intestine while varying normal load and feature size. They suggest that on smooth surfaces, a continuous mucus layer forms, leading to fluid lubrication. A surface with small patterned features may not fully penetrate the mucus layer, leading to mixed lubrication. For a surface with large patterned features, features may more intimately contact the underlying mucosa, causing boundary lubrication to predominate[31]. Modeling and experiments have shown patterning surfaces with conical frustum feature decreases work of adhesion between soft substrates and PDMS features compared to smooth PDMS[32]. Additional modeling has demonstrated that adhesion between conical frustum features and soft tissue-like substrates decreases when feature aspect ratio increases and/or spacing decreases to reduce backing layer contact[33]. Further, microscale PDMS cylindrical features have been successfully implemented as tread patterns on robotic capsule endoscopes in ex-vivo[34] and in-vivo tissue environments[35–37].

Patterned medical devices is a relatively understudied field, with limited examples such as breast implants[38,39] and hip orthoses[40,41]. Motivated by the technical challenges posed by balloon enteroscopy, we introduce a manufacturing method for single material and multi-material patterned enteroscopy balloons. We also investigate the influence of patterned feature characteristics on the anchoring of the balloon-tissue interface.

2. Material and Methods

2.1 Balloon Fabrication

A molding process was developed that allows for varied materials and patterns (Figure 2). A 3D printed clamshell mold (Grey V4 Resin, Formlabs, Somerville, MA) creates the general structure of the balloon. A central balloon mold core inserts into the center of the clamshell to form the balloon cavity. Patterned mold inserts are created separately as a flexible strip and are inserted into the inner rim of the clamshell to pattern the balloon exterior. This process allows production of balloons with patterned features molded with the balloon, compared to other methods that adhere flat patterned sheets to existing curved surfaces[36,42]. Cylindrical patterns are referred to here with the naming convention: feature radius x feature height x feature center-to-center spacing where all units are μm . All features were arranged in a hexagonal pattern and were either soft (69 kPa) or stiff (1.93 MPa) silicone. Ecoflex-30 (Smooth-On, Inc), a platinum-cure silicone elastomer, was selected as the base balloon material due to its low modulus, high failure strain, and

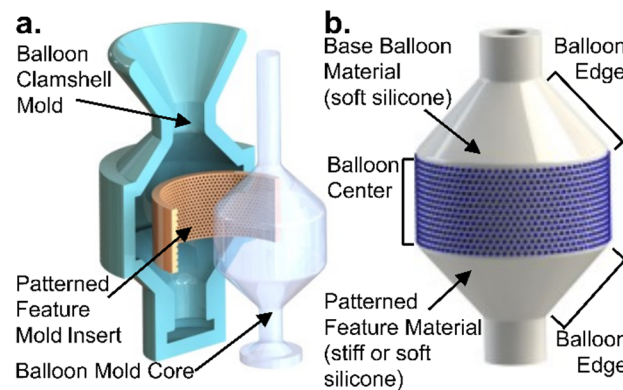


Figure 2. Balloon Manufacturing. (a) Balloons were fabricated by adding the pattern mold insert into a clamshell mold along with a mold core. Then, uncured silicone was vacuum injected into a funnel at the top of the mold, degassed, and cured. (c) The completed balloon has a base layer of Ecoflex-30 silicone with patterns along its center of either soft (Ecoflex-30) silicone or stiff (SmoothSil-960) silicone.

ease of manufacturing. Soft patterns were manufactured from Ecoflex-30. Stiff patterns were manufactured from SmoothSil-960, another higher modulus platinum-cure silicone, because it cures to Ecoflex-30. Additionally, both soft and stiff materials have been shown to be skin-safe with few effects from long-term use[43].

Patterned balloons were created using one of three methods: 1) direct 3D printing negative pattern geometry into the clamshell balloon mold, 2) reverse molding pattern inserts that were inserted into the clamshell mold (Figure 3), 3) fabrication of a positive pattern from a laser-etched Kapton mold (Potomac Photonics, Baltimore, MD), and then molding a flexible negative from PDMS that can be inserted into the clamshell mold (Figure 2a).

To fabricate single-material Ecoflex-30 (Smooth-On, Inc., Easton, PA) balloons, the clamshell was assembled so that it contained the unfilled patterned feature mold insert and balloon mold core. Next, the clamshell mold was injected with uncured Ecoflex-30 silicone and degassed under vacuum. The filled balloon mold cured at room temperature for a minimum of four hours. For the multi-material balloons, the pattern mold was separately filled with the additional material and degassed. The excess material was then scraped away, leaving the material just in the pattern. The filled pattern mold was then inserted into the clamshell mold and the balloon material was injected and cured yielding a completed balloon (Figure 3).

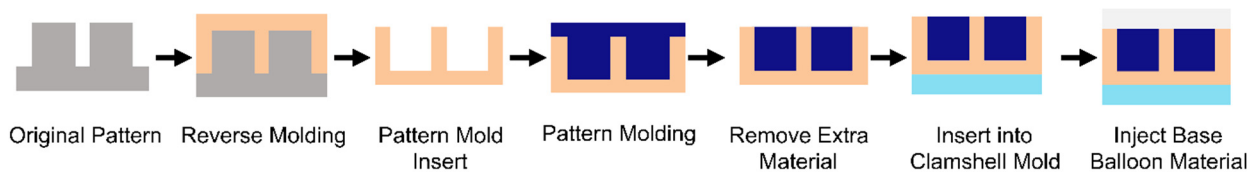


Figure 3. Balloon Manufacturing. Several patterns were created using a reverse molding protocol so that patterns can be added to a curved surface.

2.2 Pattern Geometries

Twelve types of balloons with patterned features were tested (Figure 4). Conical, dome, and cylindrical patterned features are referred to using the naming convention: radius x height x center-to-center spacing in μm . Specific features are grouped into sub-studies and discussed below. The default patterning location was the center strip of the balloon as shown in Figure 2b.

Patterns tested were divided into five areas of investigation. First, patterned feature size and scale was studied. Kwon et al found a peak in friction force of cylindrical low aspect-ratio features at a $140 \mu\text{m}$ diameter[21]. Additional work has demonstrated performance of PDMS conical frustums of this diameter in modeling and as robotic wheels in an in-vivo and ex-vivo intestine environment[32,35,44]. Therefore, $70 \times 70 \times 245$ conical frustum features were selected for this first area of investigation. $70 \times 70 \times 245$ conical frustum features were fabricated using Method 2. Larger $350 \times 350 \times 1225$ dome negatives were fabricated using Method 1. Larger features were tested because we hypothesized they may be able to penetrate the mucus layer to reach the mucosa and achieve better anchoring compared to smaller features that may remain embedded within the slippery mucus. Both soft and stiff $70 \times 70 \times 245$ conical frustums and $350 \times 350 \times 1225$ domes were investigated in one animal as a sub-study. The results of the first sub-study informed patterned features tested for subsequent sub-studies. Second, the role of feature location was also investigated in three balloon types using stiff $350 \times 350 \times 1225$ domes: the center strip (standard for other patterns), conical sides of the balloon (edge), and balloon center + edge. These patterned textures were fabricated using Method 1. Third, an additional sub-study investigated height and spacing of stiff cylindrical features: $350 \times 700 \times 1225$, $350 \times 350 \times 2450$, $350 \times 700 \times 1225$, and $350 \times 700 \times 2450$. These patterned features were fabricated with Method 3. Fourth, additional uncategorized features were tested including soft circumferential $350 \times 350 \times 1225$ ribs fabricated using Method 1 and stiff $350 \times 350 \times 1225$ cones fabricated using Method 2. Smooth silicone

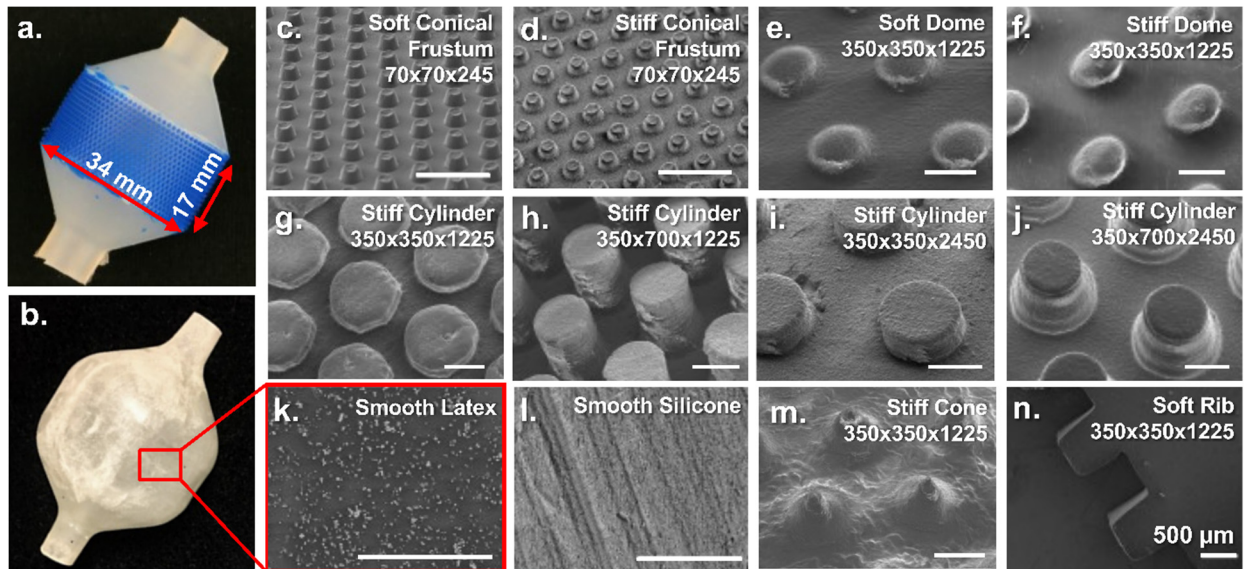


Figure 4. Balloon patterns. (a) Representative balloon molded with patterned features on the cylindrical center strip. (b) Smooth latex balloon used for balloon enteroscopy with the same dimensions as the molded balloons. Balloons in a passive, uninflated state shown in part a and b, can be deflated further by pulling a vacuum. (c-n) Scanning electron microscope images of each patterned feature tested on the molded balloons. Scale bars represent 500 μm . Patterned features have the naming convention: feature radius x feature height x feature center-to-center spacing in μm .

balloons fabricated using Method 3 with a smooth PDMS pattern mold insert. These were used as a control for all studies and are referred to here as smooth silicone (PDMS-molded) or smooth silicone in a control context. Commercially available smooth latex balloons used for endoscopies were investigated as well. Because they were made from a different material, these were not used as a control so that the effects of balloon patterned features could be isolated.

2.3 Ex-Vivo Tissue Testing

Balloons were evaluated in a porcine ex-vivo small intestine, an experimental platform that resembles the balloon's actual use. The goal of ex-vivo testing was to evaluate peak force, the maximum force it takes to dislodge an inflated balloon from a small intestine, between different patterned balloons. Peak force is suggestive of the force it takes a balloon to slip against the intestine in a clinical setting. A larger peak force is considered a more effective balloon.

To evaluate anchoring force of patterned balloons, a custom measurement system was built to hold a section of porcine intestine, inflate an inserted balloon, and pull it out while measuring force, displacement, and balloon pressure (Figure 5). Balloons were placed on a rigid acrylic tube to represent the endoscope or overtube. This tube contained a hosing piece that allowed for inflation, set to 6.5 kPa with a pressure regulator (NAR2000, SMC) and attachment to the force sensor. This pressure is similar to the maximum balloon pressure used in clinical balloon enteroscopy. A pressure sensor (MPXV6115 VC6U, NXP USA) recorded pressure inside the balloon during tests. A motor driver (2x7a Roboclaw, BasicMicro) controlled a motor (12V DC brushed motor, Pololu) attached to a reel and fishing line to pull the balloon at constant velocity and recorded displacement. A tensile force sensor (LCM100, Futek) was placed in line with the direction of balloon pull. Data were acquired with a Data Acquisition Device (MyDAQ, National Instruments) using a custom MATLAB script.

All animal procedures were performed in compliance with the appropriate Institutional Animal Care and Use Committee (facility accreditation number: 00235). Ex-vivo samples were obtained from animals used

for other studies at the facility, reducing the need to sacrifice additional animals. Each animal was placed on a gelatin diet two days before tissues were harvested, all data were collected within twelve hours of animal sacrifice, and harvested intestine was stored in phosphate buffered saline prior to testing. For each balloon tested, an approximately 30-cm segment of excised porcine small intestine was attached to the testing clamp. The balloon was inserted into the open end of the intestine sample and inflated with air to 6.5 kPa. The balloon was pulled out of the intestine sample at constant speed while force and air pressure are measured. Each individual balloon was tested ten times using one intestine sample. The intestine sample was changed between balloons. In total, tissue from six animals was used. Due to procedure length, all study procedures could not be completed in one sitting, necessitating the need for multiple animals. Two control balloons of smooth silicone were tested on each animal ($n = 12$) and two balloons of each pattern were tested except for soft 350x350x1225 ($n = 4$), stiff 350x350x1225 ($n = 8$), and smooth latex ($n = 3$).

To address variability between animals, tissue samples were not taken from any specific location along the small intestine and measured peak forces were normalized by the performance of smooth silicone balloons for each animal studied. Tissue directionality was not considered, but to the authors' knowledge no literature exists on directional contact properties of the small intestine. Smooth silicone balloons consistently demonstrated a lower peak force than all patterned balloons across all animals tested, providing a level of confidence for these assumptions.

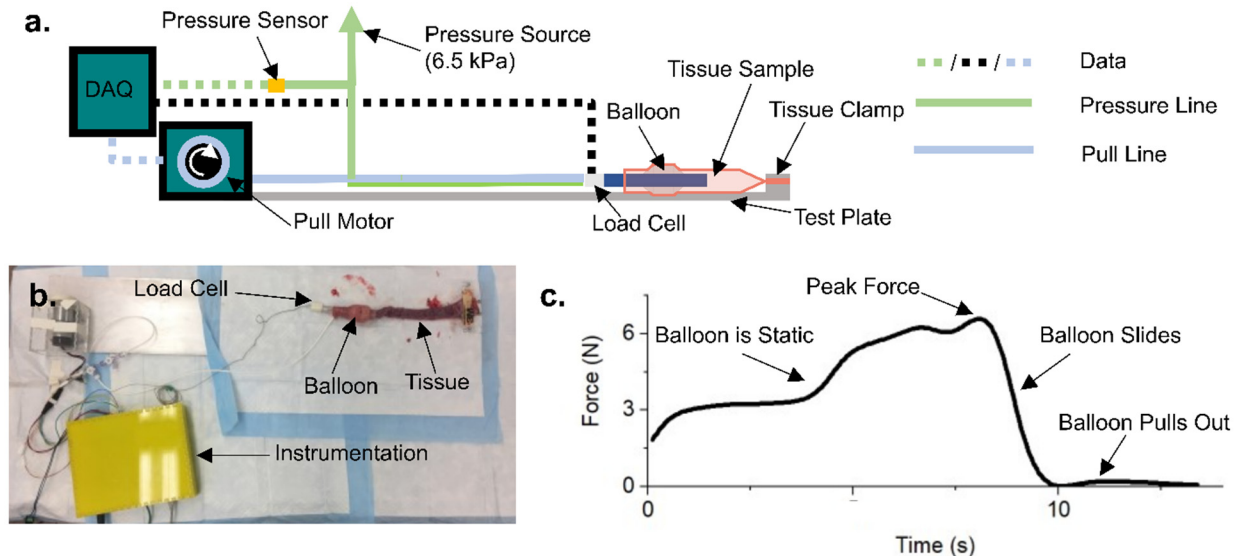


Figure 5. Ex-vivo testing. (a) Ex-vivo balloon testing device schematic. A balloon is inserted into a tissue sample clamped to a test plate. Then, the balloon is inflated from the pressure source. As the pull motor turns, the DAQ collects data from the pressure sensor and load cell. Data are recorded on a laptop computer with MATLAB. (b) Image of experimental ex-vivo balloon testing setup. (c) Representative force vs. time curve of a balloon pull test. Force is low when the motor starts turning and the balloon is static. Force rapidly increases as the motor continues turning. Peak force occurs when the balloon begins sliding. After a force plateau, force rapidly decreases as the balloon slides along the intestine. When the balloon pulls out, force returns to baseline.

2.4 Data Processing

Force data were smoothed using cubic splines and a smoothing parameter of 0.8. Peak force was the maximum force value of smoothed data. A normalization constant for each animal was created by averaging peak forces from smooth silicone balloons. All trials were divided by this constant for each animal. Normalized values were then pooled between balloons of the same pattern type. A one-way ANOVA compared peak force between balloon groups with $\alpha = 0.01$.

3. Results and discussion

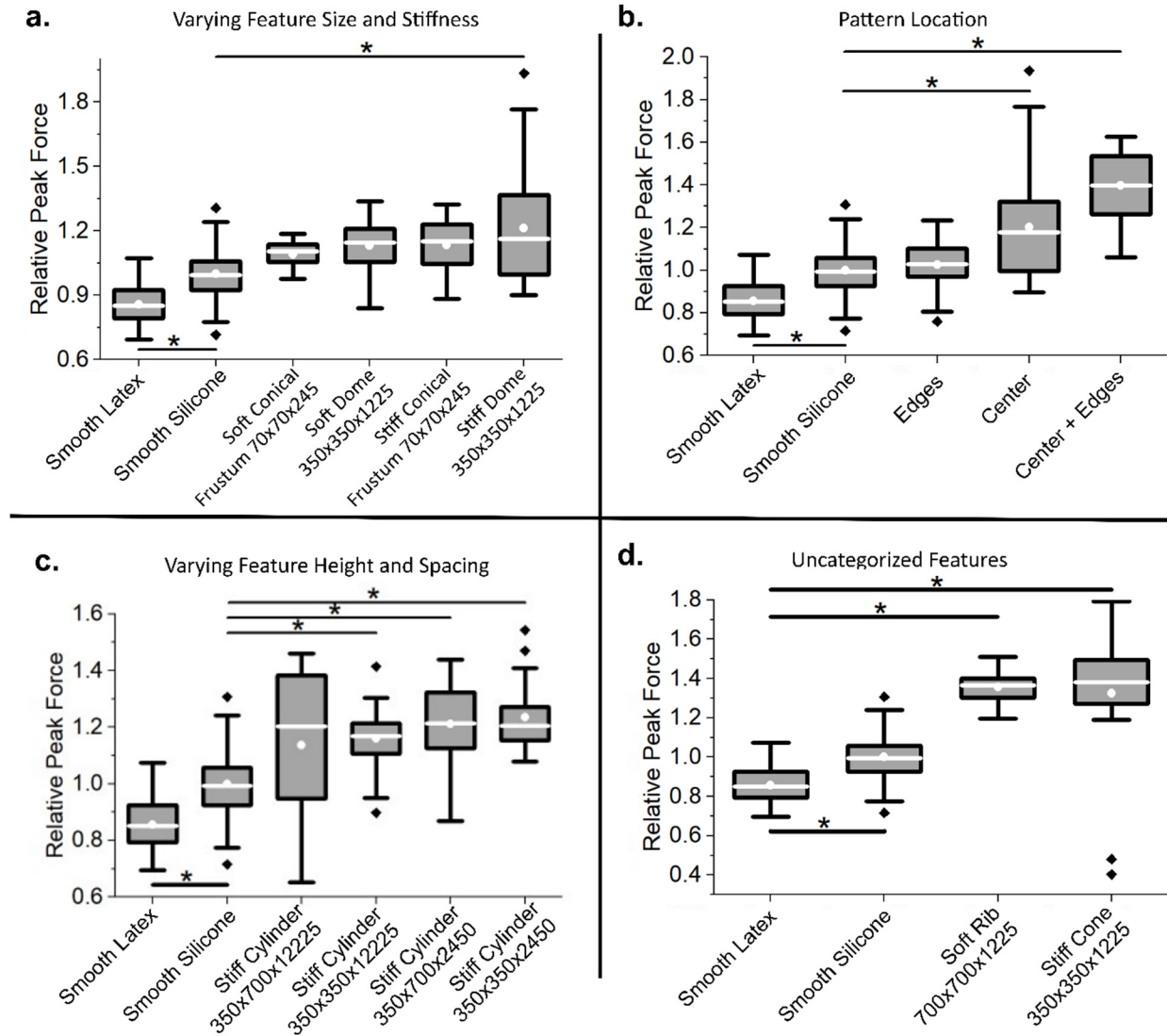


Figure 6. Results categorized by balloon type. Box and whisker plots show experimental results where the box represents the 25-75 percentile interval and whiskers show 1.5 standard deviations. The median is the near center line of the box and mean is the center white point. Outliers are black diamonds and significant differences ($p < 0.01$) are represented by black asterisks. (a) Stiff 350x350x1225 domes, stiff 70x70x245 conical frustums, and soft 350x350x1225 domes have significantly larger peak force than smooth silicone balloons. Soft 70x70x245 conical frustums do not have significantly higher peak force compared to smooth silicone balloons. (b) Center and center + edge balloons have significantly higher peak force than smooth silicone. Balloons with patterned edges do not have significantly different peak force than smooth silicone balloons. (c) All cylindrical features have similar peak force, including increased height, increased spacing, and increased height and spacing. These features all have significantly larger peak force than smooth silicone. (d) Ribs and conical features have significantly larger peak force compared to smooth silicone.

3.1 Varying Feature Scale and Stiffness

The soft and stiff silicone materials were compared in two feature types: smaller conical frustums (soft and stiff 70x70x245 conical frustums) and larger domes (soft and stiff 350x350x1225 domes). Of note, both geometries are approximately cylindrical, but differ due to manufacturing methods. Only stiff

350x350x1225 domes have significantly higher peak force compared to smooth silicone ($p = 7.00 \times 10^{-7}$). Both stiff features exhibit a higher peak force than their soft counterparts for both 70x70x245 conical frustums and 350x350x1225 domes, but this difference is not significant (Figure 6a).

These results differ from Kwon et al. and Zhang et al. who found a 70 μm feature diameter maximized friction. However, the features used in these two studies used different aspect ratios, slightly different but still cylindrical feature shapes, materials, and tissues. In this study, stiff features may penetrate better through the mucus layer of the small intestine (approximately 54 μm thick)[38] and bend less under shear loading, allowing for increased friction with the intestinal wall leading to a larger anchoring force. It is also reasonable that larger features may interface with villi of the small intestine (about 1 mm in length). Additionally, as suggested by Zhang et al., smaller features may embed in the mucus layer and experience hydrodynamic lubrication while mucus may only cover portions of larger features, resulting in boundary lubrication[31].

3.2 Varying Pattern Location of Stiff Dome Features

Most patterns were located on the center strip of the balloon (center) due to ease of manufacturing, but patterning only the conical balloon edges (edges) or the entire balloon (both the center strip and conical edges: center + edges) with stiff 350x350x1225 domes was investigated to elucidate effects of pattern location on anchoring force. Patterns that cover the entire balloon are more effective than patterns that only cover the balloon center or edges. The balloons with the largest patterned surface area, center + edge, have the highest overall peak force of any balloon ($p = 7.00 \times 10^{-7}$ compared to smooth silicone). Center + edge balloon peak force is significantly higher than the other two locations: edge ($p = 7.00 \times 10^{-7}$) and center/350x350x1225 ($p = 4.85 \times 10^{-4}$). Additionally, patterns on the center strip of the balloon contribute more to peak force than those on the angled edges of the balloons. Center/350x350x1225 patterns have significantly higher peak force than edge patterns ($p = 7.07 \times 10^{-4}$) as shown in Figure 6b.

Stiff 350x350x1225 domes demonstrate an increased peak force when they cover the entire balloon surface. Adding more total features likely leads to more contact at the pattern-tissue interface and a soft, deformable material like mucus-covered tissue may conform to the features, generating a larger peak force. However, pattern location on balloons is also important. Balloons with patterned edges have a similar peak force to smooth silicone balloons and a smaller peak force compared to balloons with patterned centers. Patterning the center strip of the balloon significantly increases peak force. This is likely due to the fact that the balloon's central region engages with tissue first during inflation and likely imposes the largest amount of pressure against the tissue wall when compared to other balloon regions.

3.3 Varying Height and Spacing of Cylindrical Features

Aspect ratio and spacing have been previously shown to affect patterned feature contact properties and were investigated in this sub-study[30–32,45]. These features include stiff 350x350x1225 cylinder, widely spaced 350x350x2450 cylinder, high aspect ratio 350x700x1225 cylinders, and high aspect-ratio and widely spaced 350x700x2450 cylinders. All cylindrical patterned features have statistically similar peak force, including taller or more widely spaced patterned features. Stiff 350x350x1225 cylinders, stiff 350x350x2450 cylinders and stiff 350x700x2450 cylinders have significantly higher peak force than smooth silicone balloons ($p = 6.41 \times 10^{-6}$, 4.83×10^{-6} , and 8.09×10^{-7} , respectively) as shown in Figure 6c.

The two 350x350x1225 features, domes, and cylinders, have similar peak forces, suggesting that the sharp edge of these larger features may not be important to balloon anchoring. The finding that all cylindrical features have similar peak force suggests that the aspect ratios and spacing in this sub-study are not critical to balloon performance. It is possible that taller features contribute to peak force up to a certain height, after

which increased height does not alter patterned feature interaction with small intestinal mucus. Increased feature spacing can potentially increase contact with the backing layer between features, leading to increased adhesion[33]. However, feature concentration per unit area decreases, potentially leading to similar true contact area and similar anchoring force in these cylindrical features.

3.4 Uncategorized Features

Additional features were studied that did not fit into any specific category. Soft rib features were investigated due to their relative ease of manufacturing. Stiff cones were investigated as an additional feature shape. Both soft rib and stiff cone features have significantly higher peak force compared to smooth silicone ($p = 7.00e-7$, $p = 7.00e-7$, respectively) as shown in Figure 5d and have some of the largest peak forces overall compared to smooth silicone. For a continuous ring, such as the soft rib, material may only flow over the tops of features as compared to discrete pillars where material may both flow over the tops of features and in between them. This could result in increased anchoring force for soft rib features. In addition, the point of the cones may create a large local stress that penetrates the mucus layer, increasing mucosal contact and increasing anchoring force.

3.5 Overall Results

In a combined analysis of sub-studies described above, all silicone balloons, apart from balloons with patterned features only on the edges, have significantly higher peak force compared to smooth latex, including smooth silicone balloons (Table 1). Seven patterned balloon types have significantly higher peak force compared to smooth silicone including soft rib, stiff center + edge, stiff cone, stiff 350x350x2450 cylinder, stiff 350x700x2450 cylinder, stiff 350x350x1225 cylinder, and stiff 350x350x1225 dome. Five balloon types do not have significantly higher peak force than soft silicone: soft 70x70x245 conical frustum, stiff 70x70x245 conical frustum, soft 350x350x1225, stiff 350x700x1225 cylinder, and edges. The overall best balloon types from the limited design space explored are center + edge stiff 350x350x1225 domes, soft ribs, and stiff cones (Figure 7).

Uninflated and inflated patterned feature morphologies differ and are further discussed in *Appendix A: Effects of Inflation on Patterned Feature Morphology*. With balloon inflation, soft and stiff 70x70x245 conical frustums become more widely spaced from each other. Soft patterned features deform more than stiff patterned features (Figure A1). Other stretched

Patterned Feature Type	Category	Performance Relative to Smooth Latex	p-value
Smooth Latex	Smooth	Very Poor	0.00764
Edges	Pattern Location	Poor	0.999
Stiff Conical Frustum 70x70x245	Varying Size and Stiffness	Poor	0.0505
Stiff Cylinder 350x700x1225	Cylindrical Features Varying Size and Spacing	Poor	0.0375
Soft Dome 350x350x1225	Varying Size and Stiffness	Poor	0.0119
Stiff Dome 350x350x1225	Varying Size and Stiffness, Pattern Location	Medium	7.00 e-7
Stiff Cylinder 350x350x1225	Cylindrical Features Varying Size and Spacing	Medium	6.41 e-6
Stiff Cylinder 350x350x2450	Cylindrical Features Varying Size and Spacing	Medium	7.83 e-6
Stiff Cylinder 350x700x2450	Cylindrical Features Size and Spacing	Medium	8.09 e-7
Center + Edges	Pattern Location	High	7.00 e-7
Cone 350x350x1225	Uncategorized	High	7.00 e-7
Rib 700x700x1225	Uncategorized	High	7.00 e-7

Performance is categorized as follows: Very Poor – significantly lower peak force compared to smooth silicone, Poor – peak force not significantly different from smooth silicone, Medium – significantly higher peak force compared to smooth silicone and mean peak force < 1.3 times that of smooth silicone, High – significantly higher peak force compared to smooth silicone and mean peak force ≥ 1.3 times that of smooth silicone. α is set to 0.01.

patterned features were not imaged, due to difficult sample preparation. However, it can be extrapolated that other patterned features exhibit similar geometric changes with stretch. In addition, due to the combined effects of patterned feature fabrication and deformation during balloon inflation, not all types of patterned features can successfully be manufactured. For example, a lower limit exists on how closely features can be spaced apart, though the fabrication techniques outlined in this work allow for production of a wide range of patterned features.

Additionally, the differing manufacturing methods and material properties of the latex versus silicone balloons may account for some differences in performance. For example, the walls of manufactured silicone balloons are thicker than those of the latex balloons though the outer dimensions are similar. Thus, smooth silicone balloons were considered the control and compared to patterned balloons. With these results, it appears clear that the addition of patterned features significantly contributes to anchoring force.

In all tests, including clinically available smooth latex balloons, visible tissue damage was observed where the tissue became dusky in color. It is unknown if these changes resemble those that occur in an in-vivo enteroscopy procedure where the small intestine has a viable blood supply. Histology should be performed during future in-vivo testing of balloons. In-vivo histology will likely give a better indication of damage compared to ex-vivo tissues undergoing degenerative changes independent of balloon damage. The presence of gross changes in all tissues during ex-vivo tests indicates patterned balloons do not cause greater damage than smooth latex balloons. Additionally, no trend in peak force was observed over the life of a tissue sample, demonstrating that using the balloons multiple times does not significantly affect peak force (Figure A1).

The ex-vivo study protocol is a first approximation to the balloon enteroscopy procedure and therefore limited in several ways. The in-vivo small intestinal contents, tissue viability, hydration, mucus, and blood supply likely change upon excision. Tissue was used within several hours of animal sacrifice and kept in a phosphate buffered saline to reduce these changes. In addition, supporting structures such as the mesentery are absent in an excised small intestine. This may change anchoring force because the tissue may be less distensible and because the in-vivo small intestine geometry is convoluted compared to straight ex-vivo segments. However, the differences found in balloon performance may translate to in-vivo evaluation. A balloon that anchors better in a straight, more deformable section of intestine will also likely anchor better in a curved, less distensible section. Future in-vivo studies should be performed to evaluate balloons in a more clinical setting.

Our study of the pattern design space finds several important factors that contribute to peak force. Stiff silicone features result in a larger peak force than features made from softer silicone. Larger features such as ribs, and 350x350x1225 cylinders, cones, and domes also demonstrate an increased peak force. Patterning the entire balloon also shows an increase in peak force. Location of patterns are important as well. For example, the center strip of the balloons contributes more than the edges of the balloons to peak force. Finally, features with continuous rings like the ribs or features with areas of stress concentration like cones have increased peak force relative to smooth balloons. By patterning balloons with discrete features, we have created a balloon with significantly greater anchoring force in the small intestine compared to smooth balloons and over 1.6 times the anchoring force of standard smooth latex enteroscopy balloons.

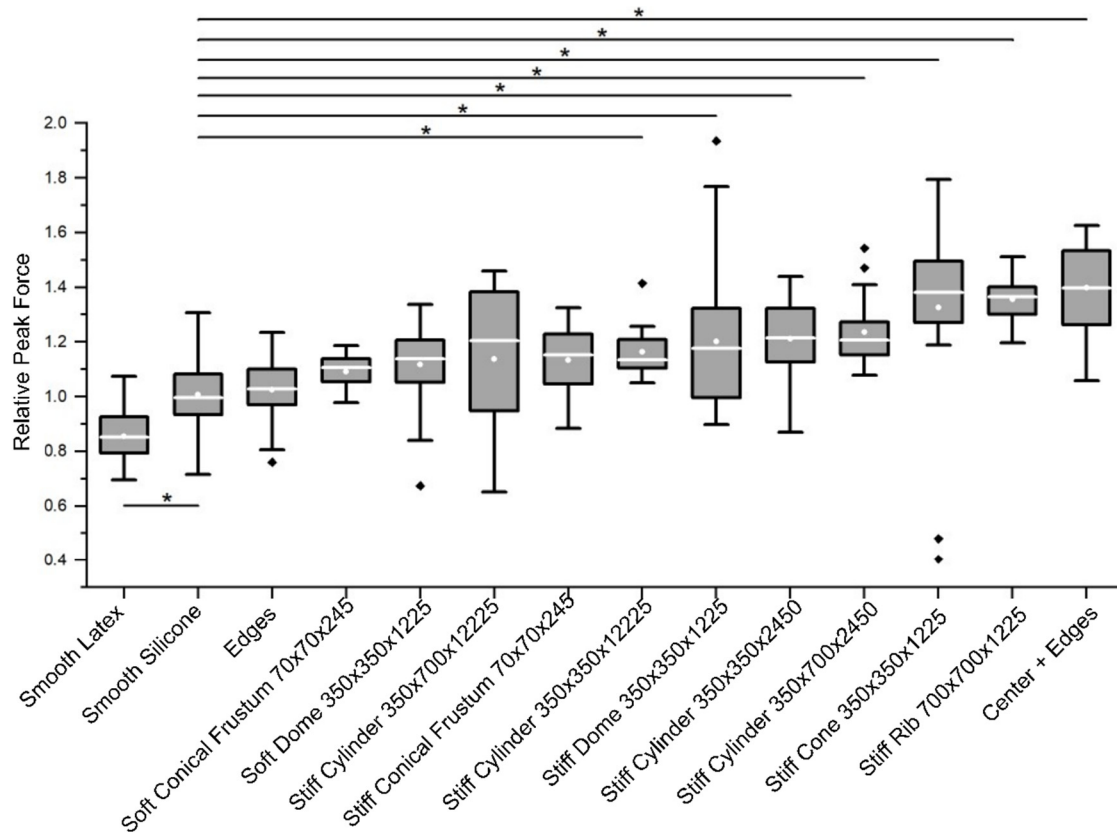


Figure 7. Normalized peak force of patterned balloons. Both smooth latex and smooth silicone balloons have significantly lower peak force than patterned balloons. Larger, stiffer, more conical patterns that cover a greater portion of the balloon’s surface tend to have greater peak force.

Conclusions

Enteroscopy balloons were fabricated with patterned features and determined larger, stiffer, conical patterns that cover a large surface area of medical balloons increase their anchoring abilities to soft, mucus-covered intestinal substrates. First, we demonstrate the ability to add patterned features to curved surfaces. Most pattern research to date is on planar surfaces[46,47] and most textured medical devices are random rough surfaces[39] or in the case of hip implants, negative dimples[40,41], making this technique an important tool for increasing the range of patterns and types of objects that can be patterned. For example, textured stents with superior anchoring could reduce migration. Patterned medical robots could benefit from application-specific contact properties. For example, medical robots utilized in the intestine could improve traction and/or locomotion against the intestine resulting from wheels or tracks with patterned features[35,37].

Second, we demonstrate that patterning balloons can increase peak force relative to smooth balloons. Stiffer, larger, conical patterns over the entire balloon surface have improved performance. Future work should focus on specific pattern attributes and the mechanisms by which patterns anchor to soft tissue.

Finally, we demonstrate improvement upon balloon enteroscopy. Additional translational studies are indicated such as balloon testing with an endoscope in-vivo where gastroenterologists can give feedback on device performance. We have overall demonstrated that the addition of patterned features to medical devices can have profound effects on their performance. With further investigation, patterned balloons could lead to more effective balloon enteroscopies, resulting in wider adoption of balloon enteroscopy procedures among gastroenterologists and improved patient outcomes.

Acknowledgements

Leah Bowen and Karl Johannes contributed equally to this work.

This research was supported in part by NSF Award 1636203, NSF Award 1827787, the Colorado Office of Economic Development and International Trade Advanced Industries. Scanning Electron Microscopy work was performed in the Colorado Shared Instrumentation in Nanofabrication and Characterization (COSINC): the COSINC-CHR (Characterization). Animal work was completed with the assistance of the Office of Laboratory Animal Resources at the University of Colorado. The authors would like to thank the Laboratory for Interdisciplinary Statistical Analysis (LISA), Department of Applied Mathematics, University of Colorado Boulder for their statistics advice.

References:

- [1] H. Yamamoto, C. Ell, H. Kita, A. May, Double-Balloon Endoscopy, in: *Video Capsul. Endosc.*, Springer Berlin Heidelberg, Berlin, Heidelberg, 2014: pp. 113–118. https://doi.org/10.1007/978-3-662-44062-9_13.
- [2] G. Ciuti, R. Caliò, D. Camboni, L. Neri, F. Bianchi, A. Arezzo, A. Koulaouzidis, S. Schostek, D. Stoyanov, C.M. Oddo, B. Magnani, A. Menciasci, M. Morino, M.O. Schurr, P. Dario, *Frontiers of robotic endoscopic capsules: a review*, *J. Micro-Bio Robot.* (2016). <https://doi.org/10.1007/s12213-016-0087-x>.
- [3] H. Yamamoto, H. Kita, K. Sunada, Y. Hayashi, H. Sato, T. Yano, M. Iwamoto, Y. Sekine, T. Miyata, A. Kuno, H. Ajibe, K. Ido, K. Sugano, *Clinical outcomes of double-balloon endoscopy for the diagnosis and treatment of small-intestinal diseases*, *Clin. Gastroenterol. Hepatol.* (2004). [https://doi.org/10.1016/s1542-3565\(04\)00453-7](https://doi.org/10.1016/s1542-3565(04)00453-7).
- [4] M. Manno, C. Barbera, H. Bertani, R. Manta, V.G. Mirante, E. Dabizzi, A. Caruso, F. Pigo, G. Olivetti, R. Conigliaro, *Single balloon enteroscopy: Technical aspects and clinical applications*, *World J. Gastrointest. Endosc.* 4 (2012) 28. <https://doi.org/10.4253/wjge.v4.i2.28>.
- [5] L.B. Gerson, J.T. Flodin, K. Miyabayashi, *Balloon-assisted enteroscopy: technology and troubleshooting*, *Gastrointest. Endosc.* 68 (2008) 1158–1167. <https://doi.org/10.1016/j.gie.2008.08.012>.
- [6] S.A. Gross, M.E. Stark, *Initial experience with double-balloon enteroscopy at a U.S. center*, *Gastrointest. Endosc.* 67 (2008) 890–897. <https://doi.org/10.1016/j.gie.2007.07.047>.
- [7] S. Mehdizadeh, A. Ross, L. Gerson, J. Leighton, A. Chen, D. Schembre, G. Chen, C. Semrad, A. Kamal, E.M. Harrison, K. Binmoeller, I. Waxman, R. Kozarek, S.K. Lo, *What is the learning curve associated with double-balloon enteroscopy? Technical details and early experience in 6 U.S. tertiary care centers*, *Gastrointest. Endosc.* 64 (2006) 740–750. <https://doi.org/10.1016/j.gie.2006.05.022>.
- [8] P.B. Cotton, P. Connor, D. McGee, P. Jowell, N. Nickl, S. Schutz, J. Leung, J. Lee, E. Libby, *Colonoscopy: Practice variation among 69 hospital-based endoscopists*, *Gastrointest. Endosc.* 57 (2003) 352–357. <https://doi.org/10.1067/mge.2003.121>.
- [9] L.B. Gerson, J. Tokar, M. Chiorean, S. Lo, G.A. Decker, D. Cave, D. BouHaidar, D. Mishkin, C. Dye, O. Haluszka, J.A. Leighton, A. Zfass, C. Semrad, *Complications Associated With Double Balloon Enteroscopy at Nine US Centers*, *Clin. Gastroenterol. Hepatol.* 7 (2009). <https://doi.org/10.1016/j.cgh.2009.07.005>.
- [10] C.W. Teshima, G. May, *Small bowel enteroscopy*, *Can. J. Gastroenterol.* (2012).
- [11] M. Pennazio, C. Spada, R. Eliakim, M. Keuchel, A. May, C.J. Mulder, E. Rondonotti, S.N. Adler, J. Albert, P. Baltes, F. Barbaro, C. Cellier, J.P. Charton, M. Delvaux, E.J. Despott, D. Domagk, A. Klein, M. McAlindon, B. Rosa, G. Rowse, D.S. Sanders, J.C. Saurin, R. Sidhu, J.M. Dumonceau, C. Hassan, I.M. Gralnek, *Small-bowel capsule endoscopy and device-assisted enteroscopy for diagnosis and treatment of small-bowel disorders: European Society of Gastrointestinal*

- Endoscopy (ESGE) Clinical Guideline, *Endoscopy*. (2015). <https://doi.org/10.1055/s-0034-1391855>.
- [12] V. Mahadevan, Anatomy of the small intestine, *Surg. (United Kingdom)*. 32 (2014) 391–395. <https://doi.org/10.1016/j.mpsur.2014.06.003>.
- [13] F.J.O. Varum, F. Veiga, J.S. Sousa, A.W. Basit, Mucus thickness in the gastrointestinal tract of laboratory animals, *J. Pharm. Pharmacol.* (2012). <https://doi.org/10.1111/j.2042-7158.2011.01399.x>.
- [14] F.J.O. Varum, F. Veiga, J.S. Sousa, A.W. Basit, An investigation into the role of mucus thickness on mucoadhesion in the gastrointestinal tract of pig, *Eur. J. Pharm. Sci.* 40 (2010) 335–341. <https://doi.org/10.1016/j.ejps.2010.04.007>.
- [15] J.K. Gustafsson, A. Ermund, M.E.V. Johansson, A. Schütte, G.C. Hansson, H. Sjövall, An ex vivo method for studying mucus formation, properties, and thickness in human colonic biopsies and mouse small and large intestinal explants, *Am. J. Physiol. - Gastrointest. Liver Physiol.* 302 (2012) 430–438. <https://doi.org/10.1152/ajpgi.00405.2011>.
- [16] A. Del Campo, C. Greiner, E. Arzt, Contact shape controls adhesion of bioinspired fibrillar surfaces, *Langmuir*. (2007).
- [17] L. Xue, J. Iturri, M. Kappl, H.J. Butt, A. Del Campo, Bioinspired orientation-dependent friction, *Langmuir*. (2014). <https://doi.org/10.1021/la502695d>.
- [18] Y. Li, J. Krahn, C. Menon, Bioinspired Dry Adhesive Materials and Their Application in Robotics: A Review, *J. Bionic Eng.* 13 (2016) 181–199. [https://doi.org/10.1016/S1672-6529\(16\)60293-7](https://doi.org/10.1016/S1672-6529(16)60293-7).
- [19] W.G. Bae, D. Kim, M.K. Kwak, L. Ha, S.M. Kang, K.Y. Suh, Enhanced Skin Adhesive Patch with Modulus-Tunable Composite Micropillars, *Adv. Healthc. Mater.* (2013). <https://doi.org/10.1002/adhm.201200098>.
- [20] Y. Wang, H. Tian, J. Shao, D. Sameoto, X. Li, L. Wang, H. Hu, Y. Ding, B. Lu, Switchable Dry Adhesion with Step-like Micropillars and Controllable Interfacial Contact, *ACS Appl. Mater. Interfaces*. (2016). <https://doi.org/10.1021/acsami.6b01434>.
- [21] E. Cheung, M. Sitti, Adhesion of biologically inspired oil-coated polymer micropillars, *J. Adhes. Sci. Technol.* (2008). <https://doi.org/10.1163/156856108X295545>.
- [22] Y. Kim, Y. Chung, A. Tsao, R. Maboudian, Tuning micropillar tapering for optimal friction performance of thermoplastic gecko-inspired adhesive, in: *ACS Appl. Mater. Interfaces*, 2014. <https://doi.org/10.1021/am5007518>.
- [23] B. He, W. Chen, Q. Jane Wang, Surface texture effect on friction of a microtextured poly(dimethylsiloxane) (PDMS), *Tribol. Lett.* (2008). <https://doi.org/10.1007/s11249-008-9351-0>.
- [24] L. Wei, K.E. Reiter, T. McElrath, M. Alleyne, A.C. Dunn, Diffraction gratings alter the surface friction of iridescent beetle cuticle against fibrous surfaces, *Biotribology*. 20 (2019) 100108. <https://doi.org/10.1016/j.biotri.2019.100108>.
- [25] R. V. Martinez, J.L. Branch, C.R. Fish, L. Jin, R.F. Shepherd, R.M.D. Nunes, Z. Suo, G.M. Whitesides, Robotic Tentacles with Three-Dimensional Mobility Based on Flexible Elastomers, *Adv. Mater.* 25 (2013) 205–212. <https://doi.org/10.1002/adma.201203002>.
- [26] S.A. Suresh, D.L. Christensen, E.W. Hawkes, M. Cutkosky, Surface and Shape Deposition Manufacturing for the Fabrication of a Curved Surface Gripper, *J. Mech. Robot.* 7 (2015) 1–7. <https://doi.org/10.1115/1.4029492>.
- [27] H. Tian, X. Li, J. Shao, C. Wang, Y. Wang, Y. Tian, H. Liu, Gecko-Effect Inspired Soft Gripper with High and Switchable Adhesion for Rough Surfaces, *Adv. Mater. Interfaces*. 6 (2019) 1900875. <https://doi.org/10.1002/admi.201900875>.
- [28] P. van Assenbergh, M. Fokker, J. Langowski, J. van Esch, M. Kamperman, D. Dodou, Pull-off and friction forces of micropatterned elastomers on soft substrates: the effects of pattern length scale and stiffness, *Beilstein J. Nanotechnol.* 10 (2019) 79–94. <https://doi.org/10.3762/bjnano.10.8>.
- [29] E.O. McGhee, S.M. Hart, J.M. Urueña, W.G. Sawyer, Hydration Control of Gel-Adhesion and Mucosal Adhesion, *Langmuir*. 35 (2019) 15769–15775.

- <https://doi.org/10.1021/acs.langmuir.9b02816>.
- [30] J. Kwon, E. Cheung, S. Park, M. Sitti, Friction enhancement via micro-patterned wet elastomer adhesives on small intestinal surfaces, *Biomed. Mater.* 1 (2006) 216–220. <https://doi.org/10.1088/1748-6041/1/4/007>.
- [31] H. Zhang, Y. Yan, Z. Gu, Y. Wang, T. Sun, Friction Enhancement between Microscopically Patterned Polydimethylsiloxane and Rabbit Small Intestinal Tract Based on Different Lubrication Mechanisms, *ACS Biomater. Sci. Eng.* 2 (2016) 900–907. <https://doi.org/10.1021/acsbiomaterials.5b00558>.
- [32] M.D. Kern, R. Long, M.E. Rentschler, A representative volume element model for the adhesion between a micro-pillared surface and a compliant substrate, *Mech. Mater.* 119 (2018). <https://doi.org/10.1016/j.mechmat.2018.01.004>.
- [33] M.D. Kern, Y. Qi, R. Long, M.E. Rentschler, Characterizing Adhesion between a Micropatterned Surface and a Soft Synthetic Tissue, *Langmuir.* 33 (2017) 854–864. <https://doi.org/10.1021/acs.langmuir.6b03643>.
- [34] L.J. Sliker, M.D. Kern, M.E. Rentschler, Preliminary experimental results and modeling for a four degree of freedom automated traction measurement platform for quantitative evaluation of in vivo robotic capsule colonoscopy mobility effectiveness, in: *Proc. - IEEE Int. Conf. Robot. Autom.*, 2013. <https://doi.org/10.1109/ICRA.2013.6631273>.
- [35] L.J. Sliker, M.D. Kern, J.A. Schoen, M.E. Rentschler, Surgical evaluation of a novel tethered robotic capsule endoscope using micro-patterned treads, *Surg. Endosc. Other Interv. Tech.* 26 (2012) 2862–2869. <https://doi.org/10.1007/s00464-012-2271-y>.
- [36] L.J. Sliker, G. Ciuti, M.E. Rentschler, A. Menciassi, Frictional resistance model for tissue-capsule endoscope sliding contact in the gastrointestinal tract, *Tribol. Int.* (2016). <https://doi.org/10.1016/j.triboint.2016.06.003>.
- [37] G. Formosa, M.J. Prendergast, S. Edmundowicz, M. Rentschler, Novel Optimization-Based Design and Surgical Evaluation of a Treaded Robotic Capsule Colonoscope, *IEEE Trans. Robot.* (2019). <https://doi.org/10.1109/TRO.2019.2949466>.
- [38] C. Randquist, Ö. Gribbe, Highly Cohesive Textured Form Stable Gel Implants, in: *Aesthetic Reconstr. Surg. Breast*, 2010. <https://doi.org/10.1016/B978-0-7020-3180-9.00025-1>.
- [39] M.B. Calobrace, M.R. Schwartz, K.R. Zeidler, T.A. Pittman, R. Cohen, W.G. Stevens, Long-term safety of textured and smooth breast implants, *Aesthetic Surg. J.* (2018). <https://doi.org/10.1093/asj/sjx157>.
- [40] S. Ghosh, D. Choudhury, T. Roy, A. Bin Mamat, H.H. Masjuki, B. Pinguan-Murphy, Tribological investigation of diamond-like carbon coated micro-dimpled surface under bovine serum and osteoarthritis oriented synovial fluid, *Sci. Technol. Adv. Mater.* (2015). <https://doi.org/10.1088/1468-6996/16/3/035002>.
- [41] T. Roy, D. Choudhury, S. Ghosh, A. Bin Mamat, B. Pinguan-Murphy, Improved friction and wear performance of micro dimpled ceramic-on-ceramic interface for hip joint arthroplasty, *Ceram. Int.* (2015). <https://doi.org/10.1016/j.ceramint.2014.08.123>.
- [42] P. Glick, S.A. Suresh, D. Ruffatto, M. Cutkosky, M.T. Tolley, A. Parness, A Soft Robotic Gripper with Gecko-Inspired Adhesive, *IEEE Robot. Autom. Lett.* 3 (2018) 903–910. <https://doi.org/10.1109/LRA.2018.2792688>.
- [43] W.J. Bae, J.B. Choi, K.S. Kim, S.J. Kim, H.J. Cho, U.S. Ha, S.H. Hong, J.Y. Lee, S.W. Kim, AB168. Evaluation of the biocompatibility of packing materials for a catheter, *Transl. Androl. Urol.* 4 (2015). <https://doi.org/10.3978/j.issn.2223-4683.2015.s168>.
- [44] M.D. Kern, J. Ortega Alcaide, M.E. Rentschler, Soft material adhesion characterization for in vivo locomotion of robotic capsule endoscopes: Experimental and modeling results, *J. Mech. Behav. Biomed. Mater.* 39 (2014) 257–269. <https://doi.org/10.1016/j.jmbbm.2014.07.032>.
- [45] Y. Tian, Z. Zhao, G. Zoghi, Y. Kim, D. Zhang, R. Maboudian, Tuning the Friction Characteristics of Gecko-Inspired Polydimethylsiloxane Micropillar Arrays by Embedding Fe₃O₄ and SiO₂ Particles, *ACS Appl. Mater. Interfaces.* 7 (2015) 13232–13237.

- <https://doi.org/10.1021/acsami.5b03301>.
- [46] G. Carbone, E. Pierro, Sticky bio-inspired micropillars: Finding the best shape, *Small*. (2012). <https://doi.org/10.1002/sml.201102021>.
- [47] D. Brodoceanu, C.T. Bauer, E. Kroner, E. Arzt, T. Kraus, Hierarchical bioinspired adhesive surfaces-A review, *Bioinspiration and Biomimetics*. (2016). <https://doi.org/10.1088/1748-3190/11/5/051001>.

Appendix A: Effects of Inflation on Patterned Feature Morphology

Soft and stiff 70x70x245 conical frustums were stretched 100% to represent balloon inflation. Stretched samples were imaged with scanning electron microscope (Figure A1). Both soft and stiff features increase spacing when stretched. Soft features deform much more than stiff features. Soft features become shorter with a central depression with stretch compared to stiff features that look similar in their unstretched and stretched state. This finding may potentially extrapolate to other patterned features where soft features deform more with balloon inflation than stiff features, though both become more widely spaced.

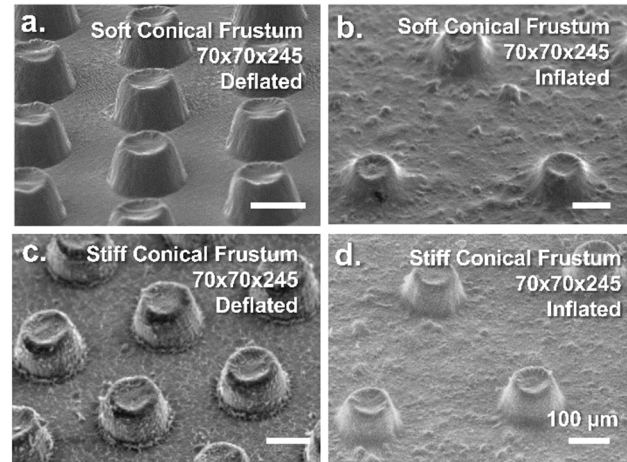


Figure A1: soft and stiff 70x70x245 conical frustums change geometry with stretch. (a) Unstretched soft conical frustums change morphology with stretch (b), becoming more widely spaced, shortening, and developing a central depression. (c) Unstretched stiff conical frustums do not change morphology with stretch (c) and only become more widely spaced.

Appendix B: Balloon Cleaning and Performance over Multiple Trials

The effect of multiple uses was studied to investigate if tissue or balloon damage affects peak force. A linear regression was fit to peak force versus trial number for each balloon. A one-sample t-test compared the regression slope and was nonsignificant. This indicates no significant linear trends with trial number were observed. A representative sample of the peak force of ten individual balloons over ten pull trials is shown in Figure A2a. Endoscopy balloons must anchor the overtube multiple times during a procedure and are not cleaned during intubation. In this case, it is ideal to have a balloon that does not lose performance with use. This data suggests that both balloons and tissue do not change with use.

A paired t-test compared peak force between pull tests where balloons were cleaned with an alcohol wipe and those that were not. Eight balloons were compared with five cleaned pull tests and five non cleaned pull tests. There is no significant difference between peak force of balloons that were cleaned with an alcohol wipe between trials and those that were not (Figure A2b). This potentially reflects a balloon's performance during its intended use. During endoscopy, balloons are not cleaned between each inflation and anchoring and it is important for balloons to retain performance even when coated with small intestinal residue.

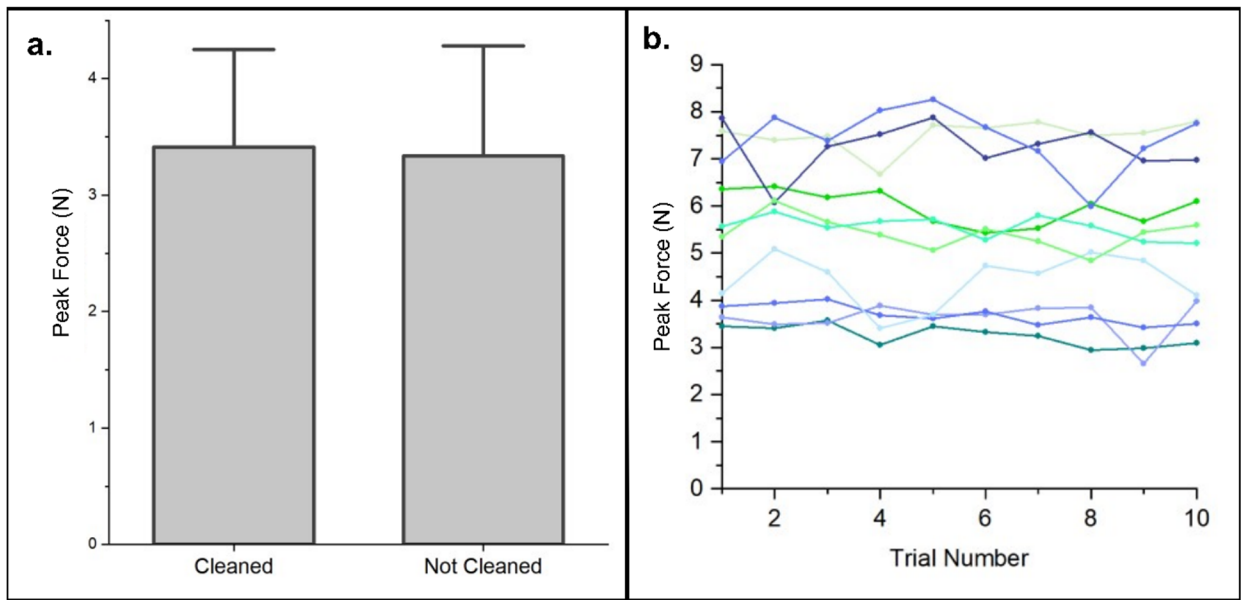


Figure A2: Balloon performance with use is consistent. (a) Cleaned and not cleaned balloons have the same peak force. Balloons have similar behavior when used multiple times. This is representative of a balloon's use in endoscopy where it will anchor multiple times during a procedure. (b) No trend is observed in balloon performance over multiple uses. A representative sample of ten individual balloons tested shows that balloons retain their anchoring properties as they are used.

Appendix C: Uninflated Balloons

Peak force between inflated smooth silicone, uninflated smooth silicone, and uninflated stiff 350x350x1225 domes are not significantly different. The only significantly higher peak forces are between inflated stiff 350x350x1225 domes and inflated and uninflated smooth silicone ($p = 7.00e-7$ and $p = 2.14e-6$, respectively). Additionally, both uninflated smooth silicone and uninflated stiff domes have statistically similar peak force compared to smooth latex peak force. This indicates patterned balloons will not have significant difficulties moving deeper into or pulling out of the small intestine at times when their anchoring properties are not needed (Figure A3).

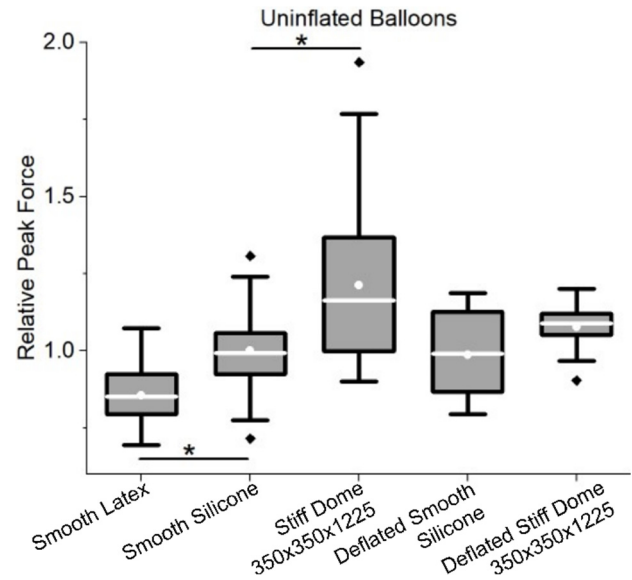


Figure A3. Comparison of peak force of inflated to uninflated balloons. Peak force of smooth silicone, deflated smooth silicone, and uninflated stiff 350x350x1225 domes were statistically similar and significantly lower than peak force of the balloons patterned with stiff 350x350x1225 domes. This indicates patterned balloons will not have significant difficulties moving deeper into or pulling out of the small intestine at times when their anchoring properties are not needed.

Appendix D: Unpatterned Balloons

An additional “rougher” smooth silicone balloon molded to a 3D-printed surface was also investigated – smooth silicone (3D print-molded). All three smooth balloons have lower peak force compared to patterned balloons. Since smooth latex had the lowest peak force compared to both smooth silicone balloons ($p = 0.00764$ for PDMS molded, $p = 0.0286$ for 3D print-molded), we can conclude that this is likely a material property of latex. Indeed, latex is observationally less “sticky” than Ecoflex-30. Both smooth silicone balloons had statistically similar peak forces. This indicates a randomly rough surface with a relatively low degree of roughness does not affect peak force (Figure A4).

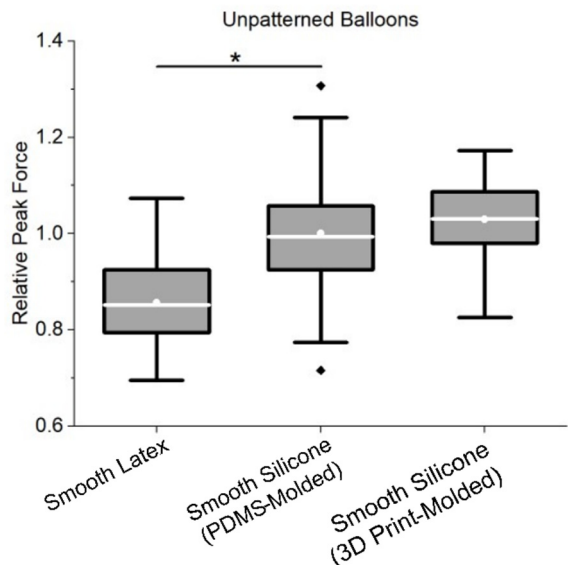


Figure A4. Comparison of smooth patterns. Both silicone patterns have similar peak forces. Both types of smooth silicone balloons have larger peak forces than the smooth latex balloons. This indicates a mildly rough surface does not affect peak force and latex balloons have the lowest performance.

Appendix E: Non-Normalized Data

Data shown in absolute peak force (Newtons) has a much larger variation than data normalized to smooth silicone balloons tested on each animal (Figure A5). A one-way ANOVA comparing absolute peak force between smooth silicone balloons shows significant differences between animals ($p = 3.325E-48$). Normalization lowers the spread of peak force values and allows for more accurate comparison of balloon performance.

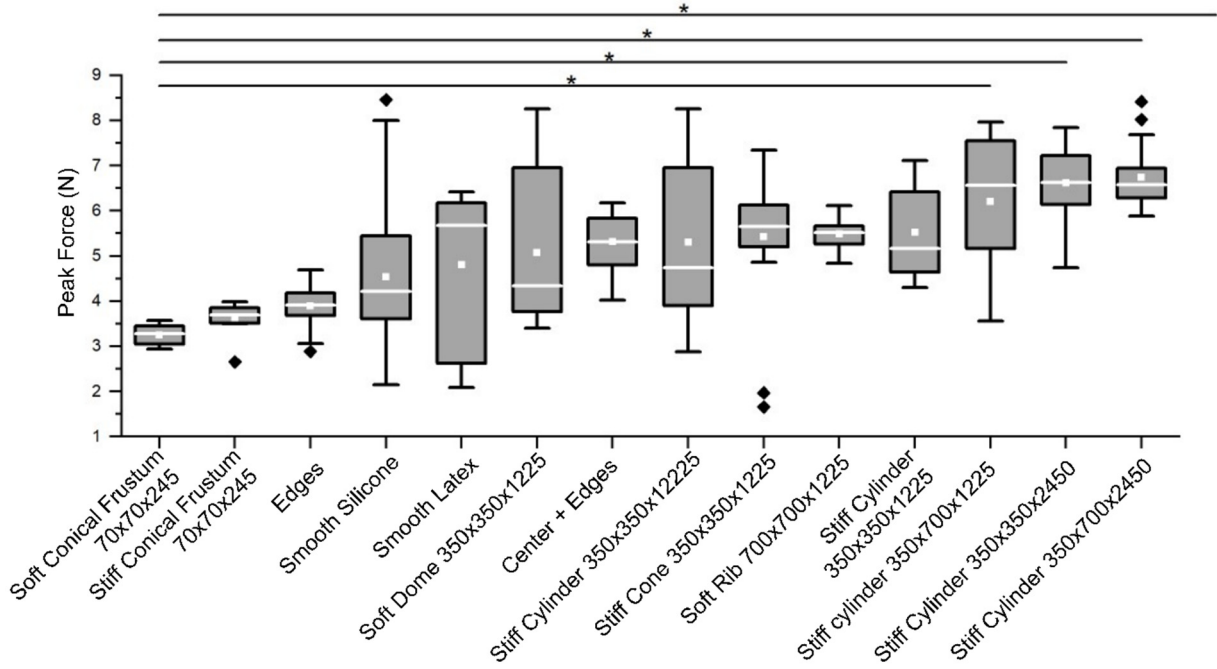


Figure A5. Pooled non-normalized results. Box plots show 25-75 percentile intervals of non-normalized results are much larger compared to normalized intervals.